

Laser induced fluorescence of the ferroelectric plasma source assisted hollow anode discharge

V. Vekselman,¹ J. Gleizer,¹ S. Yatom,¹ D. Yarmolich,¹ V. Tz. Gurovich,¹ G. Bazalitski,¹ Ya. E. Krasik,¹ and V. Bernshtam²

¹Department of Physics, Technion, Haifa 32000, Israel

²Department of Physics, Weizmann Institute of Science, Rehovot 61000, Israel

(Received 12 October 2009; accepted 23 October 2009; published online 20 November 2009)

Parameters of the plasma produced by a ferroelectric plasma source (FPS) assisted high-current (~ 1 kA), hollow anode (HA), low-pressure (10^{-4} Torr) Ar gas discharge were studied using a time- and space-resolved laser induced fluorescence (LIF) diagnostic technique. It was shown that the plasma filling of the HA cavity occurs due to the expansion of the plasma flows generated by the FPSs with a gradual time-dependent increase in the plasma density along the length of the HA cavity. These data were verified by the results of one-dimensional modeling of the plasma expansion in vacuum and time-dependent collisional-radiative modeling. Also, LIF diagnostics, which was tested on the saturation effect both experimentally and numerically, showed that the plasma ion temperature gradually increases during the discharge reaching ~ 9 eV at its end. Various phenomena (plasma kinetic instabilities, charge-exchange processes during the plasma ion interaction with the HA walls, and the model of neutral atoms ionization inside the Debye's sphere), which could be responsible for such ion temperature, were considered. © 2009 American Institute of Physics. [doi:10.1063/1.3263696]

I. INTRODUCTION

High-current (>1 kA), relativistic (>200 keV) pulsed electron beams with a duration of 10^{-7} – 10^{-5} s have found extensive applications in scientific research and industry, for instance, for pumping gaseous lasers, surface treatment, high-power microwave, and x-ray fluxes generation.^{1–3} To generate an electron beam with a moderate energy of several hundreds of keV, electron diodes with active plasma cathodes^{2,4} (i.e., when the cathode plasma is produced prior to the application of the accelerating pulse) become preferable to diodes operating with either explosive emission⁵ or flashover⁶ plasmas. The application of an active plasma cathode allows one to control the plasma parameters (density and temperature) and to generate electron beams with uniform cross-sectional electron current density distribution without time delay with respect to the beginning of the accelerating pulse. The latter becomes a problematic issue in the case of explosive or flashover plasmas when the amplitude and rise time of the accelerating electric field are <50 kV/cm and $<10^{12}$ V/(cm s), respectively.^{6,7}

A ferroelectric plasma source^{8,9} (FPS) assisted hollow anode (HA) can be considered as one of the advanced active plasma electron sources, which can be used to generate electron beams with a current density up to 30 A/cm², pulse duration up to several milliseconds, and cross-sectional area of several tens of cm².^{4,10} The FPS-assisted HA does not require additional continuous electron sources for its operation as do the plasma sources described in Refs. 4 and 11–13, where either thermionic cathode or magnetron or arc plasma sources were used to sustain hollow cathode and HA discharges.

Recent experiments^{4,10} have shown that FPS-assisted HA discharge allows reliable and reproducible plasma gen-

eration at a pressure in the range 10^{-5} – 10^{-4} Torr and a uniform current density electron beam to be extracted by applying a high-voltage pulse with an amplitude of ≤ 250 kV and pulse duration of ≤ 300 ns. It was shown that FPS-assisted HA high-current (~ 1 kA, ~ 20 μ s) discharge can be considered as a self-sustaining discharge due to the continuous formation of the FPS surface plasma, which serves as an almost unlimited electron source. The HA discharge is initiated by the formation of the plasma at the front surface of the ferroelectric sample due to incomplete surface discharges initiated at triple points of the ringlike front electrode when a nanosecond time duration, high-voltage (several kilovolts) driving pulse is applied to the rear solid electrode. Spectroscopic research showed that the density and electron temperature of the initial FPS plasma are, respectively, $n_{pi} \sim 10^{13}$ cm⁻³ and $T_e \sim 6$ eV in the vicinity of the ferroelectric surface. Thermal expansion of this plasma inside the HA leads to the beginning of the main HA high-current gas discharge supplied by an ~ 5 kV pulsed low-impedance generator. This discharge occurring between the HA walls and FPS front electrode is initiated by the current flowing through the plasma. The time delay between the formation of the FPS initial plasma and the beginning of the HA plasma discharge with a current amplitude of ~ 1 kA was found to be dependent on the background pressure and was varied in the range of 1–8 μ s for the range of pressure 5×10^{-4} – 5×10^{-5} Torr. Using spectroscopic and Thompson scattering diagnostics,^{14,15} it was found that the HA discharge initiation increases significantly the density of the surface plasma, up to $n_{pi} \sim 5 \times 10^{14}$ cm⁻³, probably due to the continuous bombardment of the FPS surface by the HA plasma ions. Here let us note that it was shown that the HA plasma obtains a positive potential of ~ 10 V with respect to the HA walls

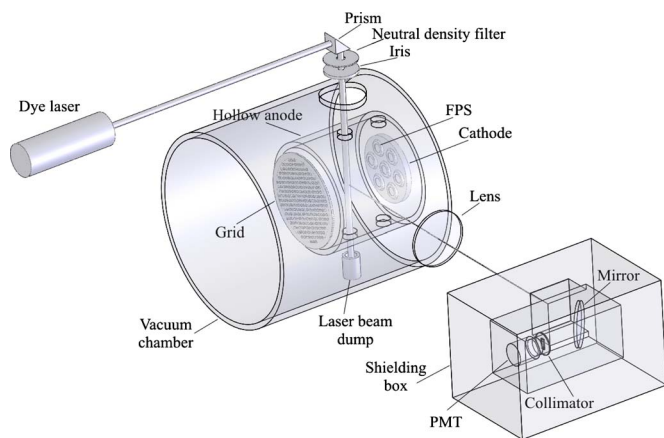


FIG. 1. (Color online) Experimental setup.

and ~ 200 V with respect to the FPS.¹⁶ It was found also that the process of dense plasma expansion inside the HA cavity occurs with a typical velocity of $\sim 10^6$ cm/s. Namely, plasma with a density of $> 10^{12}$ cm⁻³ appears in the vicinity of the HA output grid with a time delay of ~ 15 μ s with respect to the beginning of the HA discharge with a current amplitude of ~ 1 kA. In addition, it was found that the HA discharge current is sustained mostly by thermal electrons with an average temperature $T_e \sim 6$ eV. However, a fast component ($\leq 20\%$) of electrons with energy $\sim 50 \pm 20$ eV was also obtained.¹⁰ The appearance and influence of these electrons on HA bulk plasma and discharge parameters require additional research. Also, our understanding of the evolution of the HA discharge at a background pressure in the range 10^{-4} – 10^{-5} Torr is far from the clear yet.

In the present paper we characterize the FPS-assisted HA operation using time- and space-resolved laser induced fluorescence (LIF) nonperturbing diagnostics. This sensitive spectroscopic technique allows one to determine the plasma ion velocity distribution function (VDF) and plasma density evolution. The obtained results are compared with the model of the FPS plasma diffusion inside the HA cavity.

II. EXPERIMENTAL SETUP AND DIAGNOSTICS

Experiments were carried out using the HA design (see Refs. 10 and 15) at a background Ar(95%)+H₂(5%) gas pressure of $\sim 2 \times 10^{-4}$ Torr kept by two turbomolecular pumps. The HA was made of a hollow stainless-steel cylinder 25 cm in diameter with seven identical FPSs placed at the bottom of the HA cylinder on a cathode disk 10 cm in diameter (see Fig. 1). Each FPS^{8,9} was made of a ferroelectric BaTi-based ceramic sample with ring-type front and solid rear electrodes. Application of a driving pulse (~ 8 kV, ~ 200 ns) to FPSs causes plasma to form on the FPS front surfaces. Expansion of this plasma inside the HA cavity leads to the initiation of the HA discharge supplied by the PFN generator (~ 5 kV, 20 μ s). The HA outside grid was decoupled from the HA cavity by a low-inductance resistor of 50 Ω and 2 μ F capacitor connected in parallel. It was shown that such decoupling allows one to decrease the

plasma penetration through the grid significantly, due to negative autobias grid potential.¹⁰

A tunable (510–715 nm) dye laser Continuum ND6000 [spectral line full width at half maximum (FWHM) of 0.0019 nm at $\lambda = 560$ nm] pumped by a pulsed neodymium-doped yttrium aluminum garnet SureLite laser ($\lambda = 532$ nm, pulse duration of 8 ns) was used to form a laser beam with energy of 2 mJ at the desired wavelength. An iris diaphragm and a set of calibrated neutral density filters were used to attenuate the laser beam intensity and its spatial transformation. The laser beam (~ 6 mm in diameter), after its propagation through the HA plasma, was absorbed by a graphite damper placed at the bottom of vacuum chamber. A photomultiplier tube (PMT, Hamamatsu R1104) with an achromatic lens, interference filter (spectral bandpass of 5 nm at $\lambda = 461$ nm) and a set of collimators was used to collect photons emitted from the intersection volume ($5 \times 10 \times 6$ mm³) of the laser beam and plasma.

The LIF measurements were carried out using the three level Ar II scheme. A brief description of the LIF diagnostic technique is as follows. The Ar ions from the $3d^2G_{9/2}$ metastable level (lifetime $\tau > 20$ μ s) can be excited to the $4p^2F_{7/2}$ upper electronic level by absorbing laser resonant photons at $\lambda_0 = 611.492$ nm. The electrons from this upper level then spontaneously decay to the $4s^2D_{5/2}$ level by radiating fluorescence photons at 460.957 nm. By detuning the laser from the resonance wavelength the Ar ions having appropriate velocity in the direction of the laser beam can still undergo excitation to the upper level due to the Doppler effect. Indeed, for a moving ion having velocity \mathbf{V} , the resonant wavelength of transition λ^{res} in the laboratory frame, which is λ_0 in the rest frame of the moving ion, is Doppler shifted as $\lambda^{\text{res}} = \lambda_0 + \mathbf{k} \times \mathbf{V}$. Thus, neglecting the laser linewidth and assuming that the number of fluorescence photons is proportional to the population of Ar ions metastable state, one can obtain the VDF of Ar ions using the dependence of the LIF intensity on the laser wavelength, i.e., LIF excitation spectrum. If the Ar ions are in thermal equilibrium one can determine the ion temperature as well.

In fact, the above assumptions should be checked accurately in order to obtain the actual VDF of the Ar ions. Let us consider the first assumption, i.e., the effect of a finite laser bandwidth. Suppose that the population density of states 0 (metastable) and 1 (upper) are n_0 and n_1 , correspondingly. If the laser tuned at wavelength λ has a bandwidth $\delta\nu$, the velocities of absorbing ions should be in the range $\delta V = \lambda \delta\nu$ around $V = \lambda(\nu - \nu_{01})$. Here $\nu_{01} = (E_2 - E_1)/h$ is the resonant frequency of the transition $0 \rightarrow 1$, E_1 and E_2 are the energy of atomic states 0 and 1, respectively, h is the Planck constant, and ν is the laser frequency. Thus the laser finite bandwidth leads to an additional change in the state population densities n_0 and n_1 for ions with velocities in the range $[\lambda(\nu - \nu_{01}) - \lambda \delta\nu/2; \lambda(\nu - \nu_{01}) + \lambda \delta\nu/2]$. For the laser used ($\delta\nu = 1.5$ GHz) one obtains the limit in the temperature measurements of Ar species ~ 0.11 eV.

In fact, LIF diagnostics is routinely used to determine particle temperature in dc plasmas using tunable low-powerful dc lasers.^{17,18} However, for a short living (microsecond timescale) plasma one has to use a pulsed laser and

adjust both the laser pulse duration and power for proper detection of LIF photons. An excess in the laser power can lead to Stark broadening of the LIF spectrum by the laser beam electric field.¹⁹ Estimates of the Stark broadening²⁰ of the Ar II $3s^2 2p^4(^1D)4p(^2F)-3s^2 2p^4(^1D)3d(^2G)$ ($\lambda=611.492$ nm) showed that this effect becomes important at electric field >50 kV/cm, which corresponds to a power density of $\geq 10^6$ W/cm².

The most important effect that leads to a significant error in the ion temperature determination is related to large laser intensity, namely, the so-called saturation effect caused by artificial LIF spectrum broadening.²¹ This effect leads also to a nonlinear mode of LIF measurement, i.e., when the amount of fluorescence photons becomes not proportional to the population of the pumped Ar state. This effect occurs when the absorption photon rate (electron transition from state 0 to state 1) becomes almost equal to the stimulated absorption rate (electron transition from state 1 to state 0) and significantly exceeds the spontaneous rate (electron transition from state 1 to lower state 2). In this case, a further increase in the laser intensity does not lead to an increase in the spontaneous emission. Moreover, when this effect occurs at the laser spectral line wings, i.e., at $\nu \neq \nu_L$, where ν_L is the central laser frequency, one obtains artificial LIF spectrum broadening. The latter leads to the ion (atom) temperature being significantly overestimated. In order to avoid this artificial broadening, the laser intensity should be decreased. However, this results in a weaker LIF signal, which becomes comparable with the noise signal. Thus, one has to find a laser intensity, which will supply a strong LIF signal, on the one hand, and on the other will not cause artificial LIF spectrum broadening.

The optimization of the laser intensity, which allows one to avoid the saturation effect, was considered in detail in the paper by Goeckner and Goree.²¹ Using semiclassical treatment of collisionless plasma, the dependence of the FWHM of the LIF spectrum was obtained and three experimental methods were suggested to adjust the optimum laser inten-

sity. However, several misprints in Ref. 21 [for instance, there is a minus sign missing in the exponent's argument for the ion velocity distribution, and in Eq. (6) for the number of collected fluorescence photons, all powers $(-1/2)$ should be positive, otherwise a negative LIF signal is received] make the application of the expressions presented in the paper for LIF modeling problematic. Thus, following the general concept of Ref. 21, we have solved the set of rate equations for the ion distribution functions $f_i(x, V, t)$ of three ion states (0, 1, 2) involved in the LIF process mentioned above. For convenience we rewrite the set of rate equations for states 0, 1 with the same definitions as in Ref. 21:

$$\frac{d}{dt}f_0(x, V, t) = f_1(x, V, t)[A_{10} + B_{10}\Phi(x, V)] - f_0(x, v, t)\left(\frac{1}{\tau_0} + B_{01}\Phi(x, V)\right), \quad (1)$$

$$\frac{d}{dt}f_1(x, V, t) = f_0(x, V, t)B_{01}\Phi(x, V) - f_1(x, v, t)\left(\frac{1}{\tau_1} + B_{10}\Phi(x, V)\right), \quad (2)$$

where $\Phi(x, V) = 1/4\pi \int_0^{+\infty} d\nu L(\nu, \nu_{ij}, V)I(x, \nu)$ is the effective isotropic laser intensity. Here $L(\nu, \nu_{ij}, V)$ is the ion absorption spectrum, A_{ij} is the Einstein spontaneous emission coefficient, B_{ij} is the Einstein absorption coefficient, τ_i is the lifetime of the atomic state, and $I(x, \nu) = I_0[4 \ln 2 / \pi(\delta\nu)^2]^{1/2} \exp\{4 \ln 2[(\nu - \nu_i) / (\delta\nu)]^2\}$ is the laser intensity spectrum assumed to be constant during the laser pulse duration and having a Gaussian frequency distribution with a laser intensity I_0 at ν_i and bandwidth $\delta\nu$. Also, in Eqs. (1) and (2) it was assumed that the laser absorption (0–1), induced (1–0), and spontaneous (1–2) emission is the dominant process which determines the ion state 1 density population. The solutions of Eqs. (1) and (2) are

$$f_0 = -\frac{e^{-t/2(b+d)}}{2c} \left\{ C_1 e^{t/2\sqrt{b^2-2bd+d^2+4ac}}[(b-d + \sqrt{b^2-2bd+d^2+4ac})t] + C_2 e^{t/2\sqrt{b^2-2bd+d^2+4ac}}[(b-d - \sqrt{b^2-2bd+d^2+4ac})t] \right\}, \quad (3)$$

$$f_1 = C_1 e^{1/2[-(b+d)+\sqrt{b^2-2bd+d^2+4ac}]t} + C_2 e^{1/2[-(b+d)-\sqrt{b^2-2bd+d^2+4ac}]t}. \quad (4)$$

Here $a=A_{10}+B_{10}\Phi(x, v)$, $b=1/\tau_0+B_{10}\Phi(x, v)$, $c=B_{01}\Phi(x, v)$, $d=1/\tau_1+B_{01}\Phi(x, v)$. C_1 and C_2 are the coefficients, which are determined using the initial conditions for the

plasma ion Maxwell velocity distribution prior to the application of the laser pulse: $f_0(x, V, t \leq 0) = n_0 \sqrt{M/2\pi T} e^{-MV^2/2T}$, $f_1(x, V, t \leq 0) = n_1 \sqrt{M/2\pi T} e^{-MV^2/2T}$ where n_0 and n_1 are the population density of ions in states 0 and 1 and M and T are the ion mass and temperature, respectively.

The LIF photons are emitted as a result of spontaneous decay from upper state (1) to state (2). Thus, the total number of collected fluorescence photons reads

$$\begin{aligned}
N_{obs} &= \frac{d\Omega}{4\pi} A_{12} \int d^3x \int d^3v \int_0^{+\infty} dt f_1(x, V, t) \\
&= \frac{d\Omega}{4\pi} A_{12} \int d^3x \int d^3V \left[-\frac{2B_{01}\Phi(x, V)f_0(x, V, t=0) - f_1(x, V, t=0) \cdot (\lambda_2 - \lambda_1 - \alpha)}{2(\lambda_2 - \lambda_1)} e^{\lambda_1 T} \right. \\
&\quad \left. + \frac{2B_{01}\Phi(x, V)f_0(x, V, t) + f_1(x, V, t=0) \cdot (\lambda_2 - \lambda_1 + \alpha)}{2(\lambda_2 - \lambda_1)} e^{\lambda_2 T} \right]. \tag{5}
\end{aligned}$$

Here $\lambda_{1,2} = 1/2[-(b+d) \pm \sqrt{b^2 - 2bd + d^2 + 4ac}]$ are the eigenvalues of Eqs. (1) and (2) and $\alpha = b - d = (1/\tau_0) + B_{10}\Phi(x, V) - (1/\tau_1) - B_{01}\Phi(x, V)$.

Now, using Eq. (5), one can calculate the dependence of the LIF photon flux and the FWHM of the LIF spectrum on the intensity of the laser with a given bandwidth, i.e., estimate the laser power, which one requires for its nonsaturated operation. Namely, using the $n_{pl} \approx 10^{13} \text{ cm}^{-3}$ determined in our previous research (see Ref. 15) the following dependencies were calculated: (a) the dependence of the LIF photon flux on the laser intensity when the laser was turned to resonance frequency [see Fig. 2(a)] and (b) the dependence of the LIF spectrum FWHM on the laser intensity for different plasma ion temperatures [Fig. 2(b)]. The dependencies shown in Fig. 2 were used to estimate the optimum laser power as described in Ref. 21. For instance, assuming $T_i = 8 \text{ eV}$ and $T_i = 0.1 \text{ eV}$, one does not obtain artificial LIF spectrum broadening until the laser power is $\leq 3 \times 10^3$ and $\leq 30 \text{ W/cm}^2$, respectively.

To summarize, the LIF diagnostic technique is a powerful tool for pulsed plasma study, namely, for determining VDF with high time and space resolutions. However, the use of a pulsed tunable laser requires that the laser intensity be carefully adjusted in order to avoid an error in the ion VDF measurements due to artificial LIF spectrum broadening.

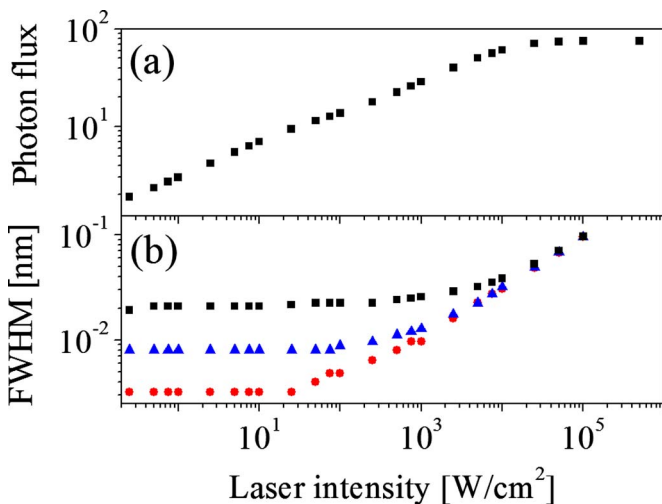


FIG. 2. (Color online) Dependencies of (a) a number of LIF photons on laser intensity at resonant wavelength of the laser and (b) FWHM of the LIF spectrum on the laser intensity for different plasma ion temperatures: (●) 0.1 eV, (▲) 1 eV, and (■) 8 eV.

III. EXPERIMENTAL RESULTS

The LIF experiments were carried out at different distances from the central FPS (3, 6, 10, and 14 cm) during the HA discharge. Typical waveforms of the HA discharge current and voltage are shown in Fig. 3, where zero time corresponds to the beginning of the FPS driving pulse.

In order to determine the LIF linear mode, experiments on laser power optimization were carried out. Experimental dependencies of the FWHM of the LIF spectrum and LIF intensity on the laser intensity at the laser resonant wavelength are shown in Fig. 4. One can see that the nonlinear mode of the LIF is realized when the laser intensity is $\sim 2.5 \times 10^3 \text{ W/cm}^2$. This agrees satisfactorily with the simulation data (see Fig. 2).

First, the LIF measurements were carried out with the dye laser tuned to the Ar II resonance transition $3d^2G_{9/2} \rightarrow 4p^2F_{7/2}$. This condition leads to the maximal LIF signal-to-noise ratio (the collected LIF photons are irradiated mostly by Ar II ions with velocities in the orthogonal plane relative to the laser beam direction). In the case of linear LIF, the temporal evolution of the fluorescence photon flux represents the plasma Ar ion density evolution. The temporal dependence of the LIF intensity during the HA discharge is shown in Fig. 5. One can see a significantly faster rise in the plasma density at $d=3 \text{ cm}$ and $d=6 \text{ cm}$ (Fig. 5, curves 2 and 3, respectively) than at $d=10 \text{ cm}$ and $d=14 \text{ cm}$ (Fig. 5, curves 4 and 5, respectively). In addition, at all tested

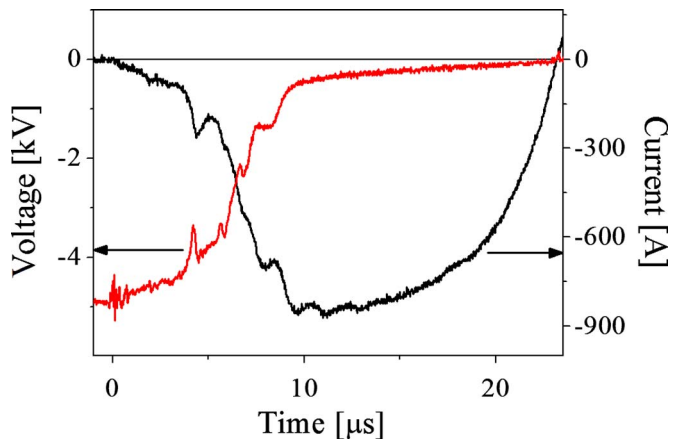


FIG. 3. (Color online) Typical waveforms of the HA discharge current and voltage. Background pressure of $2 \times 10^{-4} \text{ Torr}$.

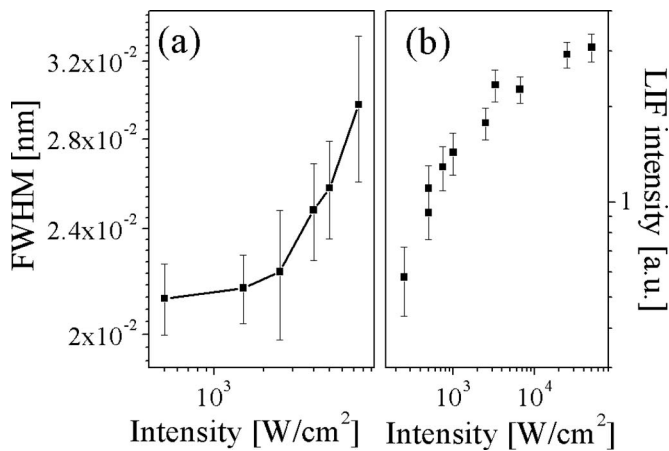


FIG. 4. Experimental dependencies of (a) FWHM of the LIF spectrum on laser intensity and (b) LIF intensity on laser intensity at the laser resonant wavelength.

distances the LIF photon flux has maximum amplitude with a decrease following it. The time delay (with respect to the beginning of the HA discharge) when the LIF photon flux reaches its maximum amplitude increases gradually with the increase in the distance d . Also, one obtains a gradual decrease in the amount of LIF photons versus the distance from the FPS, which can be associated with a decrease in the HA plasma density.

The measurements of Ar ions VDF were also performed at different distances from FPSs during the HA discharge. The summarized data are presented in Fig. 6, where the VDF were fitted by Gaussian and the “effective” temperature was introduced. The main feature of Ar ions temperature behavior is that it monotonically increases from ~ 1 eV up to 8 eV during the HA discharge.

In addition, the investigation of the LIF intensity dependence on the HA discharge current I_d (in the range 430–970 A) showed that the number of fluorescence photons is proportional to the value of I_d (see Fig. 7). These data can be explained by the increase in the HA plasma density with

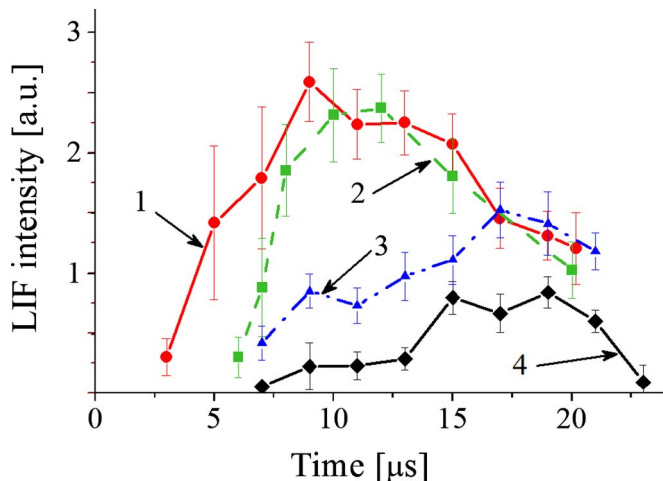


FIG. 5. (Color online) Time dependences of the LIF intensity obtained at different distances with respect to the FPS: (1) 3 cm, (2) 6 cm, (3) 10 cm, and (4) 14 cm.

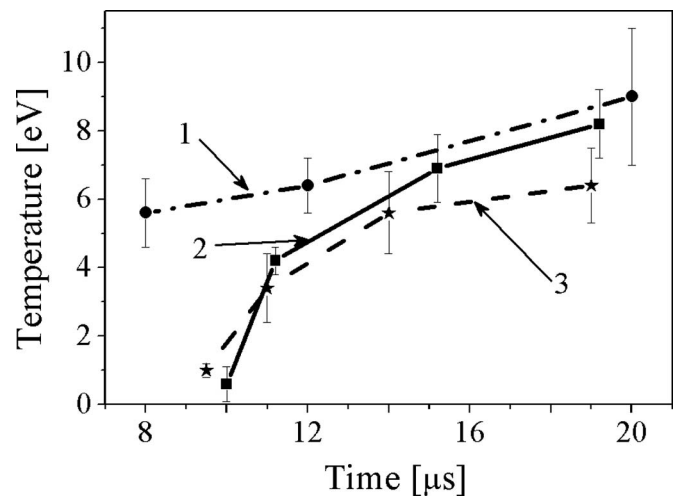


FIG. 6. Time dependence of the plasma Ar ions temperature during the HA discharge at different distances from the FPS: (1) 6 cm, (2) 10 cm, and (3) 14 cm.

the increase in I_d value, which agrees with our spectroscopic data (described in Ref. 22) and confirms the coupling between the population of upper level $4p\ ^2F_{7/2}$ and plasma density.

Finally, in order to check the LIF results concerning the high Ar II ion temperature, spectroscopic measurements were carried out as well. A 750 mm Jobin–Yvon 750M spectrometer (2400 gr/mm) with a fast ICCD camera 4Quik 04A at the spectrometer output slit was used to record the plasma spectra. However, there were several limitations in spectroscopic measurements related to spectral resolution, $0.13\ \text{\AA}/\text{pixel}$ and the large time interval of the light acquisition ($\sim 10\ \mu\text{s}$). These limitations were related to the necessity to collect sufficient light in order to obtain a reliable intensity of spectral lines. Also, because the HA plasma density decreases with the increase in the distance with respect to the FPS, these measurements were successful only at distances ≤ 30 mm. The plasma ion temperatures were obtained from the measured broadening of the C II ($6578\ \text{\AA}$)

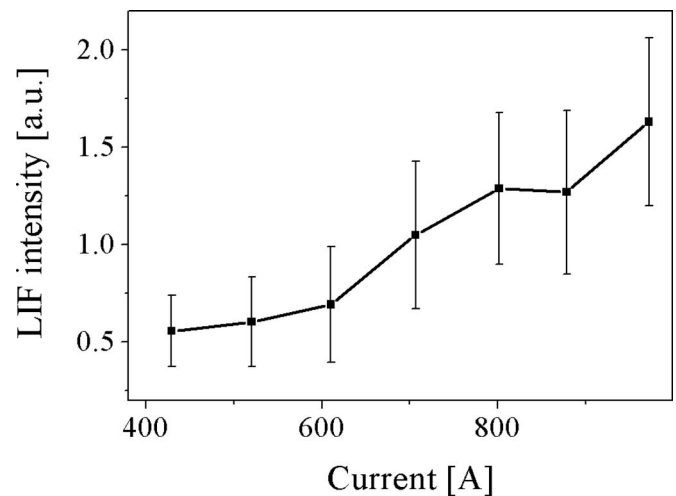


FIG. 7. Dependence of the LIF intensity vs the HA discharge current amplitude.

and Ar II (4348Å) ion spectral lines. In these experiments, a carbon thin layer was added at the front surface of the ferroelectric. It was found that C II and Ar II ion temperatures are 7.2 ± 2 and 17 ± 12 eV, respectively. Thus, one can see that the spectroscopic data also show high plasma ion temperatures. Also, one can see that the available spectral resolution of the experimental setup leads to a significant increase in the errors in ion temperature with the increase in the atomic number of element.

IV. DISCUSSION

The data presented in Fig. 5 indicate the time and space evolution of the plasma density inside the HA. Let us consider a simplified one-dimensional (1D) model of HA plasma evolution. The HA discharge triggered by the FPS plasma develops gradually with a time delay of $\tau_d \sim 8 \mu\text{s}$ with respect to the FPS plasma generation (see Fig. 2). During this transition period the density of the plasma generated by the FPSs increases up to $N_f = 2.5 \times 10^{14} \text{ cm}^{-3}$, which can be approximated as

$$N_i(t) \approx N_f \tanh[\beta(t + \tau)], \quad (6)$$

where $\tau = 1$ ns is the time constant and $\beta \approx 0.3 \mu\text{s}^{-1}$ is the parameter, which determines the asymptotic increase in $N_i(t)$ up to N_f during the first $8 \mu\text{s}$ of the HA discharge. These FPS plasma flows expand inside the HA cavity and cause ionization of Ar neutrals by the plasma electrons and fast nonthermal electrons.¹⁰ The ionized Ar atoms (Ar II) become involved in the plasma expansion, experiencing further ionization (Ar II \rightarrow Ar III). The density of Ar II ions depends on the temporal and spatial parameters of the HA plasma and nonthermal electron density and energy. Here it is assumed that the density of the Ar neutral is smaller than the density of the HA plasma, which is reasonable for the background pressure of the Ar gas (10^{-4} Torr) used in the present experiments.

Following the model described in Ref. 23, the expansion of the plasma having width $L \gg l_d$ (here l_d is the Debye length) in vacuum toward the output HA grid can be characterized by a plasma front layer, where significant deviation from quasineutrality occurs (see Fig. 8). The rear plasma boundary is located at $x=0$, namely, in the vicinity of the FPS front surface, i.e., behind the electrical sheath existing between the FPS front surface and the HA plasma where the plasma density can be estimated using Eq. (6). At the front plasma layer a negative space charge exists, which is compensated by the adjacent and rear (at the rear edge of the plasma) positive space charges. These boundary charges are responsible for the potential difference $\Delta\Phi \approx \text{Const}$ between the plasma boundaries and, respectively, for the electric field $E(t) = \Delta\Phi / [D(t + \tau)]$ in the plasma, where $D \approx \text{Const}$ is the plasma front expansion velocity. Here let us note that this electric field does not lead to a violation of the plasma quasineutrality, i.e., in the plasma bulk $n_e = \sum_i Z_i n_i$. The equation for the plasma ion motion under the electric field $E(t)$ can be written as

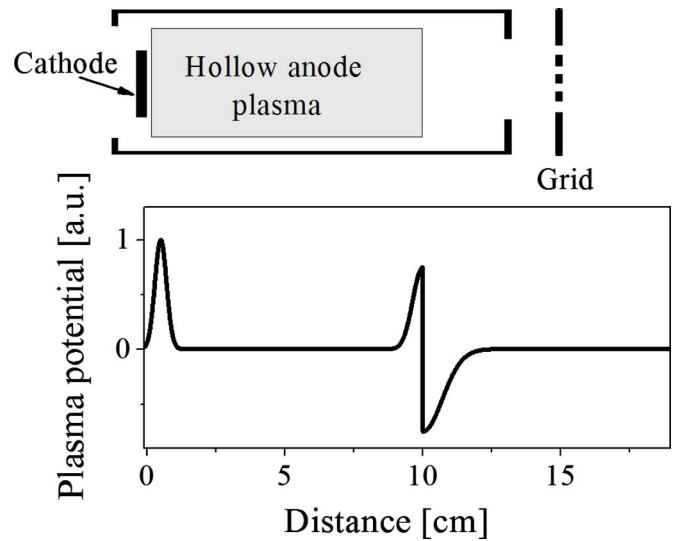


FIG. 8. (Color online) Qualitative scheme of the expanding plasma with its potential distribution.

$$\frac{\partial U}{\partial t} + U \frac{\partial U}{\partial x} = \frac{v}{t + \tau}; \quad v = \frac{e\Delta\Phi}{M_i D}. \quad (7)$$

Here e , M , and $U(x, t)$ are the charge, mass, and velocity of the plasma ions, respectively. Further it will be shown that the parameter v determines the ion velocity in the vicinity of $x=0$. The self-similarly solution of Eq. (7) can be presented as a rarefaction wave,

$$U(x, t) = v + x/(t + \tau). \quad (8)$$

Taking into account approximately conical plasma expansion, the discontinuity equation for plasma ions reads:

$$\frac{\partial[NS(x)]}{\partial t} + \frac{\partial[NUS(x)]}{\partial x} = 0. \quad (9)$$

Here $N(t, x)$ is the ion density and $S(x) = S_0 + \pi(xtg\alpha)^2$ is the cross-sectional area of the plasma flow having conical form with half divergence angle α . The solution of Eq. (9) reads:

$$N(x, t) = \left\{ \frac{S_0 N_0}{S(x)} \exp \left[- \left(\frac{x}{v(t + \tau)} \right) \right] \right\} \times \tanh \left[\beta(t + \tau) \exp \left[- \left(\frac{x}{v(t + \tau)} \right) \right] \right]. \quad (10)$$

Here let us note that this model does not consider the plasma front boundary with a typical thickness of l_d where the violation of the plasma quasineutrality occurs. The velocity of the plasma front $D \approx 10^6$ cm/s was roughly estimated using the data of the beginning of the Ar II ion spontaneous radiation at different distances from the FPS. This value of D is close to the double ion sound velocity $c_s = (T_e/M) \approx 4.5 \times 10^5$ cm/s, where $T_e \approx 8$ eV and M is the mass of the Ar ion. Concerning the plasma velocity v in the vicinity $x \approx 0$, one can suppose that, due to the adiabatically slow change in the plasma density at this location during the HA discharge, i.e., at $t > 8 \mu\text{s}$, this velocity is $v \approx c_s$. In the opposite case,

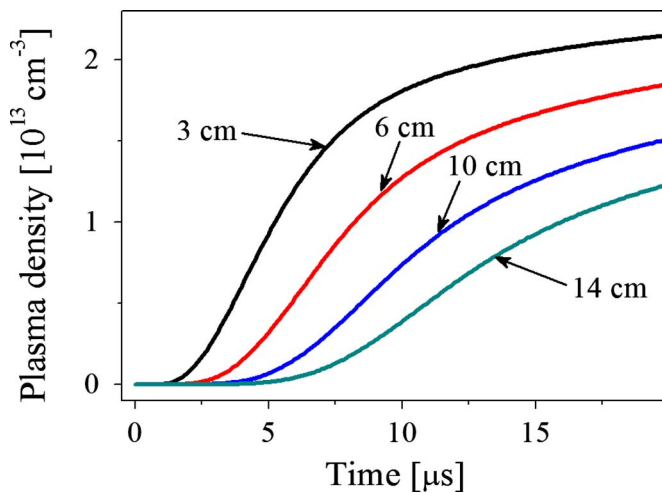


FIG. 9. (Color online) The time evolution of the plasma density at different distances from the FPS.

i.e., if $v > c_s$ or $v < c_s$, one should obtain either a decrease or an increase in the plasma density during the HA operation at this location. The equality of $v \approx c_s$ allows one to consider that the rarefaction wave, propagating in the direction $x < 0$ with velocity c_s , is transferred with velocity v toward the plasma layer front. Thus, the ion density $N(t, x \approx 0)$ is determined by the processes that govern plasma generation near the FPS [see Eq. (6)].

Results of this model, i.e., plasma density evolution inside the HA at different distances from the FPS and at different times of the HA discharge, are shown in Fig. 9. Now, using modeling results of the plasma density evolution, time-dependent collisional radiative modeling²⁴ (CRM) was carried out with regard to the Ar atoms for the plasma electron temperature in the range of $T_e = 4\text{--}8$ eV and in the presence of a nonthermal electron flux having energy in the range 40–80 eV and density in the range 10%–20% of the HA plasma density. The best fit between the CRM and experimental results was obtained for $T_e = 8$ eV and a flux of nonthermal electrons with energy of 50 ± 20 eV and density of 20% of the HA plasma density. Examples of the results of this modeling are shown in Fig. 10. Namely, the temporal evolution of Ar I, Ar II, and Ar III particles at a distance of 6 cm from the FPS are presented in Fig. 10(a) and Ar II ion temporal evolution at different distances from the FPS is shown in Fig. 10(b). One can see that the time delay in the Ar II ions' appearance, the rise in their density, and their burning (ionization) time increase with the distance from the FPS. These data agree well with the experimentally obtained data. Moreover, CRM allows one to obtain the temporal evolution of the density population of the desired atomic states, which are metastable 2G and upper 2F levels of Ar II ion in the case of the LIF scheme applied in the present research. A typical time evolution of these levels subjected to laser radiation is shown in Fig. 11 and in the inset in this figure with the increased time scale. One can see the expected drastic decrease in the population of the metastable level with a simultaneous increase in the density population of the upper level. Let us note that in a time scale of $\sim 10^{-5}$ s the density

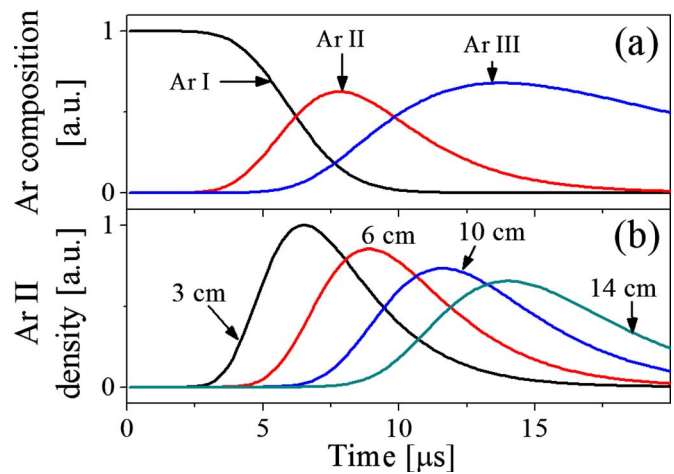


FIG. 10. (Color online) Results of CRM calculations for $T_e = 8$ eV, electron beam density of 0.2ne. (a) The time dependence of Ar I–Ar III particles relative density at a distance of 6 cm from the FPS. (b) Time dependence of Ar II ion density at different distances from the FPS.

population of 2F level already returns to its equilibrium value determined by the collision excitations process in the plasma. Based on the CRM data obtained at different time delays with respect to the beginning of the HA discharge, the temporal evolution of the population density of the upper level, i.e., the time-dependent LIF photon flux, was obtained for different distances from the FPS. The comparison between the time dependent density population of the 2F level and the experimentally obtained LIF photon flux at a distance of 6 cm from the FPS is shown in Fig. 12. One can see a good agreement between the simulated and experimental data. Thus, one can conclude that the suggested model of plasma flows generated at the surface of the FPS and expanding into the HA anode gives a correct scenario of the HA high-current discharge development. Also, the relatively fast increase in the LIF intensity at distances of 3 and 6 cm from FPSs occurs due to the overlapping of plasma flows generated by

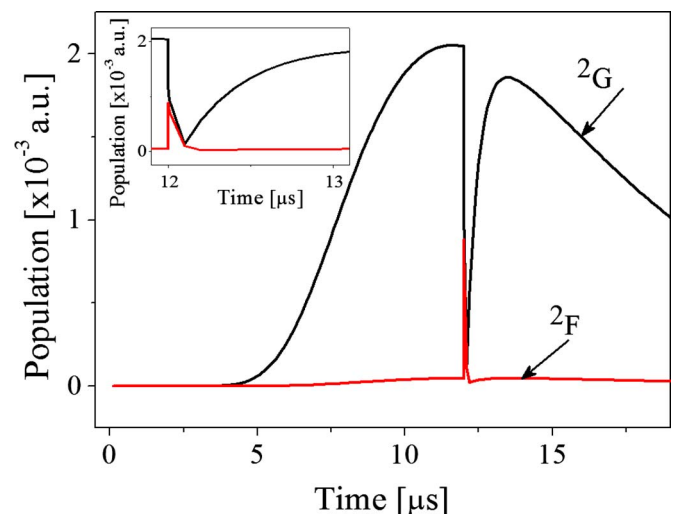


FIG. 11. (Color online) Time evolution of the population density of the metastable IIG and upper 2F levels of Ar II ion subjected to the laser radiation.

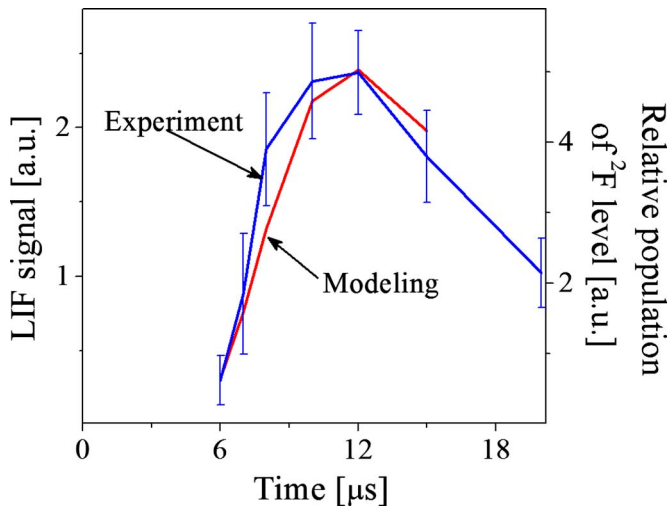


FIG. 12. (Color online) The comparison between the time dependent density population of the 2F level and the experimentally obtained LIF photon flux at a distance of 6 cm from the FPS.

individual FPSs. A rough estimate gives the growth in LIF intensity by a factor of 7 at these distances, which agrees well with the experimental data.

Now, let us discuss the ion temperature. Data obtained using LIF showed that the Ar II ion effective temperature gradually increases during the HA high-current discharge from less than 1 to 8 eV at distances ≥ 10 cm from the FPS. At smaller distances the Ar II ion effective temperature was found to be ~ 5 eV already at $\tau_d \approx 8 \mu\text{s}$ increasing up to ~ 9 eV at $\tau_d \approx 20 \mu\text{s}$. The increase in the plasma ion temperature cannot be explained by the plasma electron-ion collisions because of the too-small plasma electron-ion collision rate, which can be estimated as²⁵ $\tau_{ei} = 0.7\tau_{ee} = 2.05 \times 10^{-6} n_e T_e \ln \Lambda_e = 1.3 \times 10^{-7} \text{ s}^{-1}$ for $T_e \approx 6$ eV and plasma electron density $n_e \approx 10^{13} \text{ cm}^{-3}$, where τ_{ee} is the plasma electron-electron frequency and $\ln \Lambda \approx 10$ is the Coulomb logarithm. In the case of the Maxwellian energy distribution of electrons and ions one can estimate the equilibration time as²⁶ $\varepsilon_{eq} = (3.15 \times 10^8 A T_e) / (n_i \ln \Lambda) = 7.56 \times 10^{-4} \text{ s}$, where $n_i = n_e$ is the plasma ion density, $A = 40$ is the atomic number of Ar and T_e is measured in eV. Also, a large ion temperature cannot be explained by the fast nonthermal electron heating. Indeed, the typical time of the ion heating by “hot” electrons can be estimated as²⁷ $\tau_h \approx 17A \cdot T_{he}^{3/2} / n_e \approx 10^{-3} \text{ s}$, where T_{he} is the “hot” electron “temperature” in $^{\circ}\text{K}$ degrees.

At present we do not know the exact phenomena (phenomenon), which govern(s) plasma ion heating during the HA high-current discharge, and additional research is required. For instance, searching for electric fields (amplitude and frequency spectrum) in the HA plasma can be a key issue in determining the mechanism governing the plasma ion heating. Below, we will qualitatively and briefly consider some of these phenomena, which may lead to the high plasma ion “temperature” that was obtained.

Let us start with kinetic plasma instabilities, which can arise in the current-carrying plasma in the presence of a non-thermal electron beam. In such plasma one can consider fast arising beam instability with a nanosecond timescale incre-

ment [$\gamma \leq \omega_p (n_e/n_p) [V_e^2 / (\Delta V)^2]$, where n_e is the density of the electron beam and V_e is the electron beam velocity].²⁸ This instability occurs due to resonance energy exchange between the beam electrons having a velocity distribution $df/dV(V = \omega/k) > 0$ and the plasma wave with phase velocity $V < V_e$, where ω and k are the frequency and wave number of the plasma wave, respectively. This instability leads to the electron beam bunching and, respectively, the plasma wave energy density increasing up to $E^2/4\pi \sim n_e m_e V_e (n_e/n_p)^{1/3} \approx 1.5 \times 10^{14} \text{ eV/cm}^3$, where m_e is the electron mass. The dissipation of the plasma wave energy leads to the plasma ion heating up to ~ 10 eV. Approximately the same results can be obtained in the case of the Buneman instability²⁹ [the increment $\gamma \leq 0.69\omega_p (m_e/m_i)^{1/3}$ of this instability rise time is also in the nanosecond time scale] when one considers current-carrying plasma electrons with average velocity exceeding that of the plasma ion.

Other kinetic instabilities typical for the current-carrying plasma are the ion acoustic and parametric instabilities.^{28,30–33} The ion acoustic instability, which has a qualitative explanation similar to that of beam instability, is realized when the plasma electron current velocity ($V_{ec} = j_e/en_e$) is less than the plasma thermal velocity V_{Te} but exceeds ion sound velocity $c_s = (kT_e/m_i)^{1/2}$. This type of instability with an increment in $\gamma = \omega(m_e/m_i) \times [(V_{ec}/c_s)\cos\phi - 1]$, where ϕ is the angle between the direction of the current carrying electrons’ velocity and the direction of the ion-sound wave propagation, leads to plasma ion heating due to Landau damping of the ion-sound waves on plasma ions when the phase velocity of the ion-acoustic wave becomes comparable with V_{ec} . The saturation of this instability occurs when the plasma ions acquired velocity equals ion sound velocity. A parametric instability occurs due to nonlinear interaction between low frequency ion-acoustic and high-frequency Langmuir plasma waves. This type of instability, which also can be realized in our current-carrying plasma (low frequency ion acoustic instability) with nonthermal electron beam (high-frequency Langmuir plasma waves), could be a reason for the large ion temperature.

The other phenomenon, which also could be responsible for the increase in the ion temperature, is the charge exchange of the plasma ions when they interact with the HA walls. In our earlier research¹⁶ it was shown that the plasma acquires a positive potential of ~ 10 V with respect to the HA walls. Thus, during the HA discharge inside the sheath formed between the plasma and the HA walls there is an emission of ions with energy $E_i \approx 10$ eV from the plasma boundary toward the walls. According to the data presented in Ref. 32, during the interaction with the walls, almost all plasma ions capture electrons and reflect back toward the plasma as neutrals with energy $\sim 0.8 E_i$. These neutrals will be neutralized by the plasma electrons within the first few hundreds of nanoseconds (see Fig. 9), thus increasing the “effective temperature” of the HA plasma ions.

Finally, let us consider a simple model, which gives a straightforward explanation of the large ion temperature as well. In the case of the plasma density $n_i = 10^{13} \text{ cm}^{-3}$, an average distance between two ions is $r_i = (3/4\pi n_i)^{1/3} \approx 0.3 \mu\text{m}$ and the Debye radius $r_D = 740(T_e/n_e)^{1/2} \approx 6 \mu\text{m}$.

Thus the location of the Ar atom can be considered in the range $r_0=0.1 \mu\text{m} \leq r \leq r_i$, where r_0 is the radius of the Ar neutral atom. In the case of ionization due to collisions with the plasma electrons, the Ar ion acquires an average potential energy $\langle U \rangle = (r_i)^{-1} \int_{r_0}^{r_i} U(r) dr = [e^2 \ln(r_i/r_0)] / 4\pi\epsilon_0 r_i$. When this potential energy is transferred to the kinetic energy of the ion, the latter acquires a velocity of $\approx 5 \times 10^5$ cm/s, which is close to ion sound velocity c_s . This estimate considers that the mass of the neighboring ion, i.e., the nearest ion with respect to the Ar II ion, is significantly larger than the Ar II ion mass. In the case of ion mass equality, the Ar II ion velocity will be $(2)^{1/2}$ times smaller than c_s and significantly smaller than c_s in the case of light neighboring ions. The FPS generated plasma consists of different ions including ions with $A > 100$.²² It is reasonable to consider that ions with smaller mass will diffuse and fill the HA cavity faster than the ions with larger mass. Thus, at the beginning of the HA discharge one obtains a smaller Ar II ion effective temperature, which gradually increases when the heavy ions fill the HA cavity.

V. CONCLUSIONS

Experimental research of the HA high-current discharge using time- and space-resolved pulsed LIF diagnostics revealed that the plasma filling of the HA cavity occurs due to expansion of the plasma flows generated by the FPS. The obtained LIF data showed a gradual time-dependent increase in the plasma density along the length of the HA cavity. These data were verified by the results of 1D modeling of the plasma expansion in vacuum and time-dependent CR modeling, which includes the presence of the nonthermal electron beam. Thus, it was shown that, indeed, FPS can be considered an almost unlimited source of the plasma, allowing one to operate HA discharge at a low background pressure in microsecond and millisecond time scales without applying additional plasma sources.

Also, pulsed LIF diagnostics, which was tested on the saturation effect both experimentally and numerically, showed that the HA plasma ion temperature gradually increases during the HA discharge, reaching ~ 8 eV at the end of the discharge. Different phenomena, which could be responsible for such an unusually large ion temperature, were considered, namely, several plasma kinetic instabilities, charge-exchange processes during plasma ion interaction with the HA walls, and a simple model of neutral atom ionization inside the Debye's sphere. However, additional research related to electric field amplitude and frequency determination is strongly required in order to clarify the nature of this high plasma ion temperature.

ACKNOWLEDGMENTS

We wish to thank Evgeny Stambulchik for fruitful discussions and comments. This research was supported by the BSF (Grant No. 2006373).

- ¹A. S. Gilmour, Jr., *Microwave Tubes* (Artech House, Norwood, 1986) and references therein.
- ²E. Oks, *Plasma Cathode Electron Sources* (Wiley-VCH, Weinheim, 2006).
- ³J. Reece Roth, *Industrial Plasma Engineering* (IOP, Bristol, 1995).
- ⁴Ya. E. Krasik, D. Yarmolich, J. Z. Gleizer, V. Vekselman, Y. Hadas, V. Tz. Gurovich, and J. Felsteiner, *Phys. Plasmas* **16**, 057103 (2009) and references therein.
- ⁵G. A. Mesyats, *Explosive Electron Emission* (URO, Ekaterinburg, 1998).
- ⁶Ya. E. Krasik, J. Z. Gleizer, D. Yarmolich, A. Krokmal, V. Ts. Gurovich, S. Efimov, J. Felsteiner, V. Bernshtam, and Yu. M. Saveliev, *J. Appl. Phys.* **98**, 093308 (2005) and references therein.
- ⁷Ya. E. Krasik, A. Dunaevsky, A. Krokmal, J. Felsteiner, A. V. Gunin, I. V. Pegel, and S. D. Korovin, *J. Appl. Phys.* **89**, 2379 (2001).
- ⁸G. Rosenman, D. Shur, Ya. E. Krasik, and A. Dunaevsky, *J. Appl. Phys.* **88**, 6109 (2000) and references therein.
- ⁹G. A. Mesyats, *Phys. Usp.* **51**, 79 (2008).
- ¹⁰J. Z. Gleizer, D. Yarmolich, V. Vekselman, J. Felsteiner, and Ya. E. Krasik, *Plasma Devices Oper.* **14**, 223 (2006).
- ¹¹D. M. Goebel and R. M. Watkins, *Rev. Sci. Instrum.* **71**, 388 (2000).
- ¹²V. I. Gushenets, N. N. Koval, V. S. Tolkachev, and P. M. Schanin, *Tech. Phys.* **69**, 62 (1999).
- ¹³A. Krokmal, J. Z. Gleizer, Ya. E. Krasik, J. Felsteiner, and V. I. Gushenets, *J. Appl. Phys.* **94**, 44 (2003).
- ¹⁴D. Yarmolich, V. Vekselman, J. Z. Gleizer, Y. Hadas, J. Felsteiner, and Ya. E. Krasik, *Appl. Phys. Lett.* **90**, 011502 (2007).
- ¹⁵D. Yarmolich, V. Vekselman, J. Z. Gleizer, Y. Hadas, J. Felsteiner, V. Bernshtam, and Ya. E. Krasik, *Plasma Devices Oper.* **15**, 115 (2007).
- ¹⁶J. Z. Gleizer, A. Krokmal, Ya. E. Krasik, and J. Felsteiner, *J. Appl. Phys.* **94**, 6319 (2003).
- ¹⁷R. A. Stern and J. A. Johnson, *Phys. Rev. Lett.* **34**, 1548 (1975).
- ¹⁸S. Jun, H. Y. Chang, and R. McWilliams, *Phys. Plasmas* **13**, 052512 (2006).
- ¹⁹H. R. Griem, *Spectral Line Broadening by Plasmas* (Academic, New York, 1974).
- ²⁰E. Stambulchik, Weizmann Institute of Science (private communication).
- ²¹M. J. Goeckner and J. Goree, *J. Vac. Sci. Technol. A* **7**, 977 (1989).
- ²²A. Krokmal, J. Z. Gleizer, Ya. E. Krasik, D. Yarmolich, and J. Felsteiner, *J. Appl. Phys.* **96**, 4021 (2004).
- ²³P. Mora, *Phys. Rev. Lett.* **90**, 185002 (2003).
- ²⁴Yu. V. Ralchenko and Y. Maron, *J. Quant. Spectrosc. Radiat. Transf.* **71**, 609 (2001).
- ²⁵D. Diver, *A Plasma Formulary for Physics Technology and Astrophysics* (Wiley-VCH, Berlin, 2001).
- ²⁶Yu. P. Raiser, *Gas Discharge Physics* (Springer, Berlin, 1997).
- ²⁷L. A. Arzimovich, *Controllable Thermonuclear Reactions* (Fizmatgiz, Moscow, 1961) (in Russian).
- ²⁸L. A. Arzimovich and P. Z. Sagdeev, *Plasma Physics for Physicists* (Atomizdat, Moscow, 1979) (in Russian).
- ²⁹B. M. Smirnov, *Introduction to Plasma Physics* (Nauka, Moscow, 1982), p. 166 (in Russian).
- ³⁰F. F. Chen, *Introduction to Plasma Physics and Controlled Fusion*, 2nd ed. (Plenum, New York, 1984).
- ³¹B. B. Kadomzev, *Plasma Turbulence*, (Academic, New York, 1965), Chap. 4A; A. Galeev and R. Z. Sagdeev, in *Reviews of Plasma Physics*, edited by M. A. Leontovich (Consultant Bureau, New York, 1979), Vol. 7, pp. 1–180.
- ³²A. S. Kingsep, K. V. Chukbar, and V. V. Yan'kov, in *Reviews of Plasma Physics*, edited by B. B. Kadomzev (Consultant Bureau, New York, 1990), Vol. 17.
- ³³C. F. Barnett and M. F. A. Harrison, *Applied Atomic Collision Physics Plasmas* (Academic, New York, 1984), p. 338.